Drug Design, Development and Therapy

Dovepress
Taylor & Francis Group

Open Access Full Text Article

ORIGINAL RESEARCH

Active Ingredients and Potential Mechanism of Additive Sishen Decoction in Treating Rheumatoid Arthritis with Network Pharmacology and Molecular Dynamics Simulation and Experimental Verification

Jinhong Ren, Ze Liu, Xiaoming Qi, Xiangda Meng, Linglin Guo, Yating Yu, Tao Dong, Qingshan Li

Shanxi Key Laboratory of Innovative Drug for the Treatment of Serious Diseases Basing on the Chronic Inflammation, College of Traditional Chinese Medicine and Food Engineering, Shanxi University of Chinese Medicine, Jinzhong, People's Republic of China

Correspondence: Qingshan Li, Email sxlqs0501@sxtcm.edu.cn

Background: Rheumatoid arthritis (RA) is a chronic inflammatory autoimmune disease in which macrophages produce cytokines that enhance inflammation and contribute to the destruction of cartilage and bone. Additive Sishen decoction (ASSD) is a widely used traditional Chinese medicine for the treatment of RA; however, its active ingredients and the mechanism of its therapeutic effects remain unclear.

Methods: To predict the ingredients and key targets of ASSD, we constructed "drug-ingredient-target-disease" and protein–protein interaction networks. Gene ontology and Kyoto Encyclopedia of Genes and Genomes enrichment analyses were performed to explore the potential mechanism. The activity of the predicted key ingredients was verified in lipopolysaccharide-stimulated macrophages. The binding mode between the key ingredients and key targets was elucidated using molecular docking and molecular dynamics simulation.

Results: In all, 75 ASSD active ingredients and 1258 RA targets were analyzed, of which kaempferol, luteolin, and quercetin were considered key components that mainly act through inflammation-related pathways, such as the PI3K-AKT, TNF, and IL-17 signaling pathways, to ameliorate RA. Transcriptome sequencing suggested that kaempferol-, luteolin-, and quercetin-mediated inhibition of glycolysis reduced the lipopolysaccharide-induced production of proinflammatory factors. In vitro experiments indicated that kaempferol, luteolin, and quercetin decreased Glut1 and LDHA expression by diminishing PI3K-AKT signaling to inhibit glycolysis. Molecular dynamic simulation revealed that kaempferol, luteolin, and quercetin stably occupied the hydrophobic pocket of PI3Kδ.

Conclusion: Our results show that the PI3Kδ-mediated anti-inflammatory responses elicited by kaempferol, luteolin, and quercetin are crucial for the therapeutic efficacy of ASSD against RA.

Keywords: Autoimmune disease, traditional Chinese medicine, glycolysis, inflammation, PI3K-AKT

Introduction

Rheumatoid arthritis (RA), a chronic inflammatory autoimmune disease that affects approximately 1% of the population worldwide, is characterized by painful, swollen joints that can severely impair physical function and quality of life.[1,2] The immunopathogenesis of RA spans decades, beginning with the loss of self-tolerance, which is marked by the production of autoantibodies against post-translationally modified protein antigens. After a prolonged period of asymptomatic autoimmunity, tissue tolerance fails and synovial inflammation ensues as defective DNA repair and rewired metabolic networks drive T-cell maldifferentiation toward highly proliferative, tissue-invasive, proinflammatory effector T cells. The transition of synovial stromal cells into autoaggressive effector cells converts synovitis from acute to chronic destructive, which erodes the cartilage and bone.[3]

Received: 14 September 2024
Accepted: 14 January 2025
Published: 21 January 2025

Macrophages play an important role in RA pathogenesis. Compared with the normal synovium, biopsy specimens from patients with RA contain more macrophages.[4] These cells make up almost the entire synovial lining, and their numbers considerably increase in the sublining tissue.[4] The degree of synovial macrophage infiltration is positively correlated with the progression of joint destruction.[5,6] During the course of RA, synovial macrophages function as antigen-presenting cells, driving pathogenic T-cell infiltration, and produce cytokines (eg, IL1B, IL6, TNF-α, and IL23) to perpetuate inflammation by recruitment and activation of additional immune cells. Synovial macrophages also directly differentiate to mature osteoclasts under specific microenvironment conditions. In addition, inflammatory macrophages can produce angiogenic factors (eg, vascular endothelial growth factor (VEGF), transforming growth factor, and TNF-α) and degrading enzymes (eg, MMPs, namely MMP1, 3, 7, 10, 12, 14, and 25), which participate in the hypervascularization and articular surface erosion observed in RA, respectively.[5,7] Importantly, all agents currently used in the clinics for the treatment of RA, including conventional synthetic (cs)-, biologic (b)-, and targeted synthetic (ts)-disease-modifying antirheumatic drugs (DMARDs), and even corticosteroids, quantitatively or qualitatively affect the synovial macrophage components, directly or indirectly.[7] The decrease in the number of synovial macrophages is a validated biomarker of the clinical efficacy of antirheumatic treatment.[8,9] Therefore, synovial macrophages are clearly linked to the initiation, progression, severity, and response to RA treatment.

Sishen decoction (SSD), a well-known traditional Chinese medicine prescription, was first recorded in "YanFang Xin Bian" of the Qing Dynasty and has been used clinically to treat arthritis for hundreds of years. SSD comprises five traditional herbs: *Astragalus membranaceus* (AM), *Lonicera japonica* (LJ), *Polygala tenuifolia* (PT), *Dendrobium nobile* (DN), and *Cyathula officinalis* (CO). Additive SSD (ASSD), additionally contains *Polygonum cuspidatum* (PC) and *Hedyotis diffusa* (HD), and has a good therapeutic effect against RA. However, its main active ingredients and the molecular mechanism underlying its effect against rheumatic diseases remain poorly understood. In this study, using network pharmacology, we constructed "drug-ingredient-target-disease" and protein–protein interaction (PPI) networks to predict key ingredients and key targets of ASSD against RA, and then used databases to performed Gene Ontology (GO) and Kyoto Encyclopedia of Genes and Genomes (KEGG) pathway enrichment analyses to predict the potential mechanisms underlying the therapeutic effect of ASSD against RA. Next, we verified the predicted results using lipopolysaccharide (LPS)-stimulated macrophages. Finally, molecular docking and molecular dynamics simulation were conducted to elucidate the binding mode of key ingredients and targets. A bioinformatics analysis of GSE datasets was performed to evaluate the role of key targets in RA patients. A flowchart of the study is shown in Figure 1.

Materials and Methods

Reagents and Chemicals

RAW 264.7 cells were purchased from the Cell Culture Centre, Chinese Academy of Medical Sciences & Peking Union Medical College (Beijing, China). Kaempferol, luteolin, and quercetin were purchased from Must Bio-technology (Chengdu, China). CAL101 was purchased from Beyotime (Shanghai, China). Antibodies against pAkt (T-308) and Akt were purchased from Cell Signaling Technology (Danvers, MA, USA). Antibodies against Glut 1, c-Myc, and Ldha were purchased from Abcam (Cambridge, MA, USA).

Data Preparation

The Traditional Chinese Medicine Systems Pharmacology Database (TCMSP; http://ibts.hkbu.edu.hk/LSP/tcmsp.php)[10] and the Bioinformatics Analysis Tool for Molecular Mechanism of Traditional Chinese Medicine (BATMAN-TCM; http://bionet.ncpsb.org/batman-tcm/)[11] were used to identify the chemical ingredients of ASSD. Based on absorption, distribution, metabolism, and excretion (ADME), the ADME-related properties, including oral bioavailability (OB) ≥ 30% and drug likeness (DL) ≥ 0.18, were employed to screen the active ingredients of ASSD with favorable pharmacokinetic properties. Potential targets of the active ingredients were predicted by integrating genes collected from TCMSP, BATMAN-TCM, and SwissTargetPrediction (http://www.swisstargetprediction.cn/).[12]

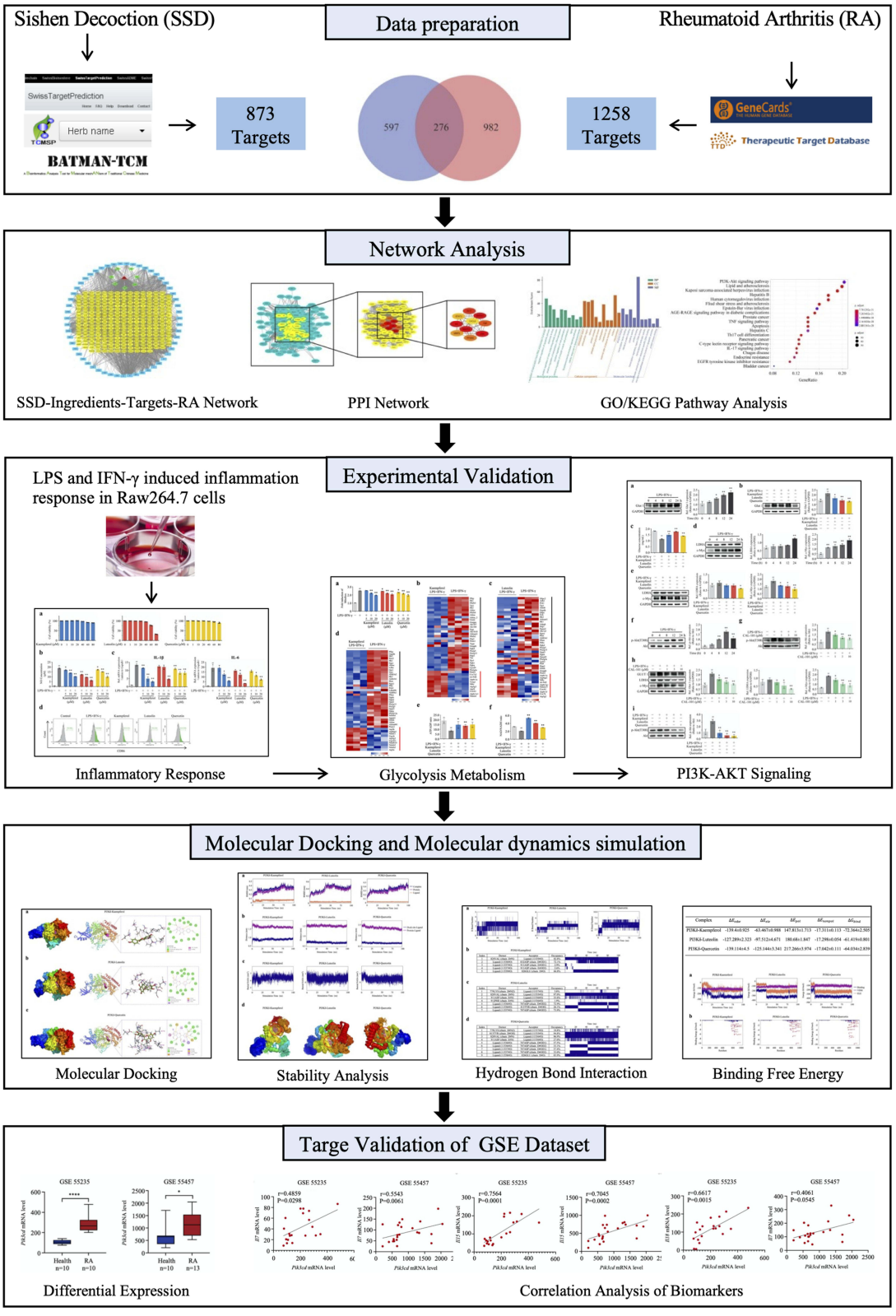

Figure 1 Flow chart of the present study.

https://doi.org/10.2147/DDDT.S489323

Genecards (http://www.genecards.org/)[13] and Therapeutic Target Database (TTD, http://database.idrb.cqu.edu.cn/TTD/)[14] were used to identify RA-related targets in *Homo sapiens*. The target database of ASSD-treated RA was established by comparing and analyzing the overlapping targets between the RA-related and active ingredient-related targets.

Network Construction

The ASSD-ingredients-targets-rheumatoid arthritis network was created by inputting the bioactive ingredients and ASSD-treated RA targets into Cytoscape (http://cytoscape.org/).[15] Nodes represent the ingredients and targets, whereas edges indicate the interactions of the ingredients and targets.

The PPI network was derived based on STRING database (http:// string-db.org/).[16] The results of the analysis using the STRING database were imported into the Cytoscape software to draw the visualized network. Clusters were obtained by analyzing the PPI network using the MCODE and cytoHubba plug-ins of Cytoscape.

GO and KEGG Pathway Enrichment Analysis

The Database for Annotation, Visualization and Integrated Discovery (DAVID) (http://david.abcc.ncifcrf.gov)[17] and the KEGG database (http://www.kegg.jp/)[18] were used to perform GO and KEGG enrichment analyses of SSD-treated RA targets, respectively. Statistical significance was set at $P < 0.05$.

Cell Culture

RAW 264.7 cells were cultured in Dulbecco's modified Eagle's medium (DMEM; Gibco, NY, USA) supplemented with 10% fetal bovine serum (Gibco, NY, USA). The cells, after reaching approximately 80% confluence, were pretreated with kaempferol, luteolin, or quercetin for 30 min, and then incubated with LPS (100 ng/mL) and interferon-γ (IFN-γ, 20 ng/mL) for 24 h.

Cell Viability Assay

The cytotoxicity of kaempferol, luteolin, and quercetin on RAW 264.7 cells was assessed using the Cell Counting kit-8 (CCK-8; Boster, Wuhan, China). The cells were seeded in 96-well plates at a density of 2×10^4 cells/well. The next day, cells were treated with kaempferol, luteolin, or quercetin at the indicated concentrations. After 24 h of incubation, the CCK-8 solution was added to each well and the plate was incubated for 4 h. The absorbance at 450 nm was measured using a SpectraMax i3x spectrophotometer (Molecular Devices, CA, USA).

Measurement of Nitric Oxide (NO) Levels

NO levels were measured using the Griess reagent based on the accumulation of nitrite and nitrite reductase. Equal volumes of Griess reagent I and II (Beyotime) were mixed with the culture supernatant in enzyme-labeled plates. The absorbance at 540 nm was measured using the SpectraMax i3x spectrophotometer (Molecular Devices).

Measurement of Il1b and Il6 Levels Using Quantitative Real-Time PCR

Total RNA was extracted from the cells using the TRIzol reagent (Takara, Tokyo, Japan) according to the manufacturer's instructions. cDNA was synthesized using a reverse-transcription kit in a 20 μL reaction mixture (Takara, Tokyo, Japan). Gene expression levels were quantified using SYBR Premix Ex Taq (Takara) on a 7900HT Real-Time PCR system (Applied Biosystems, MA, USA). The mRNA levels of target genes were normalized against those of *GAPDH*. The primers for the target genes were synthesized at Sangon Biotech Co. Ltd. (Shanghai, China). The sequences of the primers were as follows: Il1b forward: 5′-TGCCACCTTTTGACAGTGATG-3′ and Il1b reverse: 5′-TGATGTGCTG CTGCGAGATT-3′; Il6 forward: 5′-GGGACTGATGCTGGTGACAA-3′ and Il6 reverse: 5′- TGCCATTGCAC AACTCTTTTC-3′.

Measurement of Cd86 Levels Using Flow Cytometry

Cells were blocked with anti-mouse CD16/32 antibody (BioLegend, San Diego, CA, USA) before staining with an anti-mouse CD86-PerCP/Cy5.5 antibody (BioLegend, CA, USA). After washing, the cells were analyzed using a CytoFLEX S cytometer (Beckman Coulter, CA, USA). All data were analyzed using CytExpert according to the manufacturer's instructions.

Measurement of Mitochondrial Reactive Oxygen Species (ROS)

Mitochondrial ROS levels were assessed using a MitoSox probe (Yeasen, Shanghai, China). The cells were incubated with the MitoSox dye at 37 °C for 30 min. Thereafter, the medium was aspirated and the cells were quickly washed twice with phosphate-buffered saline to remove the unbound dye. Images were captured at 580 nm using an ImageXpress Micro Four High-Content Imaging System (Molecular Devices). For quantitation of intensity, images from 27 sites in three wells per experiment were analyzed using the MetaXpress analysis software.

RNA Sequencing

Total RNA was isolated and purified using the TRIzol reagent (Invitrogen) following the manufacturer's instructions. Poly (A) RNA was purified from total RNA using Dynabeads Oligo (dT) 25–61005 (Thermo Fisher, CA, USA) and fragmented into small pieces using the Magnesium RNA Fragmentation Module (catalog# e6150; NEB, USA). The cleaved RNA fragments were reverse-transcribed into cDNA using SuperScript II Reverse Transcriptase (catalog# 1896649; Invitrogen, USA), which were used to synthesize U-labeled second-stranded DNA with *Escherichia coli* DNA polymerase I (catalog# m0209; NEB), RNase H (catalog# m0297; NEB), and dUTP Solution (catalog# R0133; Thermo Fisher). Single- or dual-index adapters were ligated to the fragments and size selection was performed using AMPureXP beads. After treatment of the U-labeled second-stranded DNA with heat-labile UDG enzyme (catalog# m0280; NEB), the ligated products were amplified using PCR. Finally, 2×150 bp paired-end sequencing (PE150) was performed on an Illumina NovaSeq 6000 (LC-Bio Technology Co., Ltd., Hangzhou, China) following the manufacturer's protocol.

Measurement of NAD^+/NADH and ATP/ADP Ratios

The ATP/ADP ratio was measured using an ADP/ATP Ratio Assay Kit (Dojindo Laboratories, Kumamoto, Japan). The cells were plated in white 96-well plates and treated as required. ATP and ADP working solutions were added to each well, according to the manufacturer's instructions. Absorbance was detected using a SpectraMax i3x spectrophotometer (Molecular Devices).

The NAD^+/NADH ratio was measured using an NAD^+/NADH Assay Kit (Beyotime). The cells were lysed in a lysis solution. The lysates were centrifuged at 12,000 rpm for 5 min, and the supernatants were collected. Subsequently, the NAD^+ and NADH concentrations were measured according to the manufacturer's instructions.

Measurement of Glucose Consumption

To measure glucose consumption after treatment with LPS and kaempferol, luteolin, or quercetin, the culture medium was replaced with fresh medium before treatment and collected 24 h later. The glucose levels in the culture medium were measured using a glucose assay kit (Beyotime).

Measurement of the Expression Levels of Glut1, Ldha, and c-Myc and Phosphorylation of AKT Using Western Blot Analysis

Cells were lysed in RIPA buffer (50 mm Tris-HCl, pH 7.4, 150 mm NaCl, 1% NP-40, and 0.5% sodium deoxycholate) containing a Complete Protease Inhibitor Cocktail and Phosphatase Inhibitor Cocktail (Roche, Basel, Switzerland). The lysates were centrifuged at 12,000 rpm for 15 min and the proteins were quantified using a BCA protein assay kit (Boster, Wuhan, China). Total proteins were resolved using sodium dodecyl sulfate-polyacrylamide gel electrophoresis and subsequently transferred onto a polyvinylidene difluoride membrane. The membranes were incubated with specific primary and secondary antibodies. Images were acquired using the Amersham Imager 600 (Cytiva, DC, USA).

Molecular Docking and Molecular Dynamics Simulation

The crystal structure of PI3Kδ was obtained from the RCSB Protein Data Bank (PDB ID 7LQ1). The 3D structures of kaempferol, luteolin, and quercetin were downloaded from the PubChem database. Autodock Vina was used to analyze molecular docking between PI3Kδ and the small molecules. The free binding energy was obtained as an indicator to

reflect the binding, and the docking conformation with the highest output score was considered to be the binding conformation for subsequent molecular dynamics simulation.

Molecular dynamics simulation was performed by Gromacs 2022. Before simulation, the small molecules were described by the GAFF2 small molecule force field, whereas the PI3Kδ protein was described by the AMBER14SB force field, along with the TIP3P solvent box. Molecular dynamics simulation commenced with constant number, volume, and temperature (NVT) and constant number, pressure, and temperature (NPT) equilibration runs, each lasting 100 ps at 298 K. Subsequently, a 100 ns molecular dynamics simulation of the complex system was executed, with configurations saved every 10 ps. The binding free energy of the small molecules with PI3Kδ was calculated using the molecular mechanics Poisson–Boltzmann surface area (MM/PBSA).

Statistical Analysis

Data were analyzed using Prism (GraphPad Software) and are presented as the mean values ± standard deviation (SD). Differences between groups were statistically analyzed using two-tailed Student's *t*-tests. Statistical significance was set at $P < 0.05$.

Results

Data Preparation

To identify the active ingredients of ASSD using TCMSP and BATMAN-TCM, the classical ADME parameters, OB and DL, were used for screening. A total of 75 active ingredients in the formula were screened, 20 from *A. membranaceus*, 23 from *L. japonica*, 5 from *P. tenuifolia*, 6 from *D. nobile*, 4 from *C. officinalis*, 10 from *P. cuspidatum*, and 7 from *H. diffusa*. Among these, five active ingredients (kaempferol, quercetin, β-sitosterol, stigmasterol, and luteolin) were duplicated. Detailed information on the active ingredients is provided in Supplementary Tables 1 and 2. The active ingredient-related targets were retrieved from TCMSP, BATMAN-TCM, and SwissTargetPrediction, and 873 targets were obtained after overlapping. The data of active ingredient-related targets are shown in Supplementary Tables 1 and 2.

A total of 1258 RA-related targets were obtained from Genecards and TTD. Using a Venn diagram of RA-related and active ingredient-related targets, 276 common targets were filtered as the target database of ASSD-treated RA (Figure 2).

ASSD-Ingredients-Targets-RA Network and Key Ingredients

To evaluate which ASSD ingredients are critical to RA treatment, the ASSD-ingredients-targets-RA network was built using the Cytoscape software by converting the 75 active ingredients and 276 common targets to nodes. As shown in Figure 3, the network consists of 365 nodes and 1795 edges. Among them, kaempferol (edges =84), luteolin (edges =96),

Figure 2 Venn diagram of 873 additive Sishen decoction (ASSD) and 1258 rheumatoid arthritis (RA) targets showing an overlap of 276 targets.

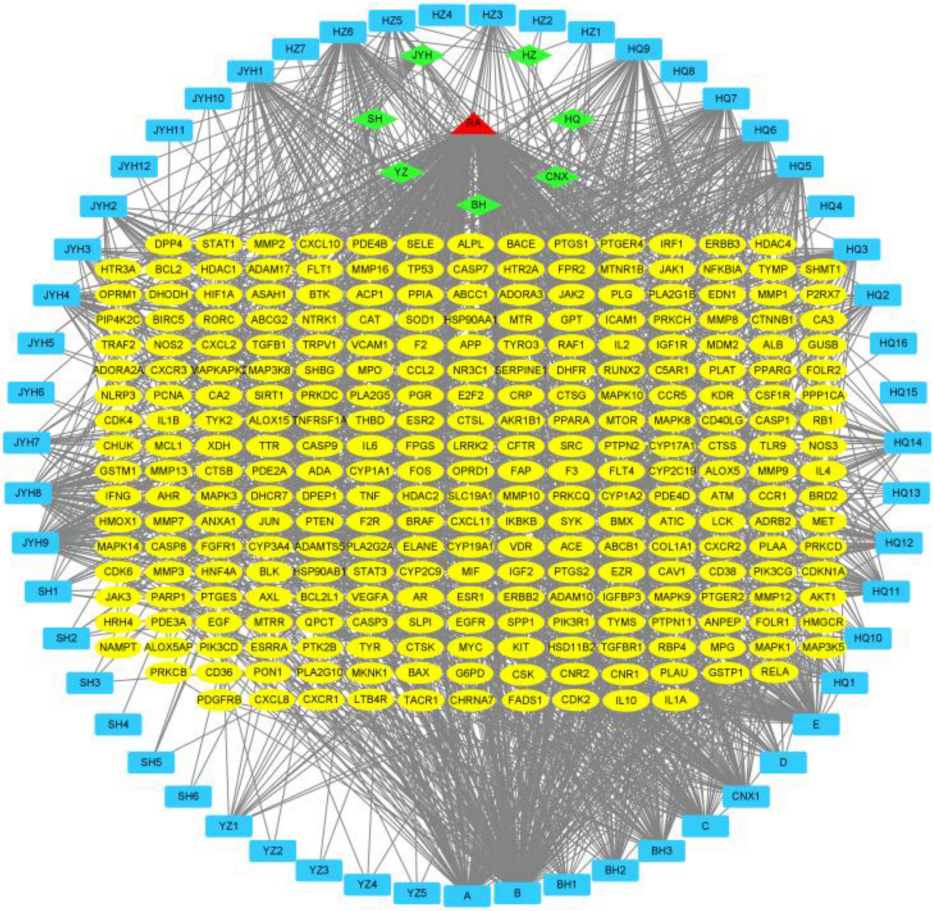

Figure 3 The ASSD-ingredients-targets-RA network. The green rhombuses represent 7 traditional herbs in additive Sishen decoction (ASSD), blue rectangles represent the active ingredients in 7 traditional herbs, and yellow ellipses represent 276 potential targets in ASSD-treated rheumatoid arthritis (RA).

and quercetin (edges =155) were closely linked to the targets, suggesting that these compounds are the key ingredients for the therapeutic effect of ASSD against RA.

PPI Network and Key Targets

To further explore the underlying targets of ASSD protection against RA, a PPI network for the 276 common targets, with 7794 edges was constructed using the STRING database and Cytoscape software. By analyzing the network using MCODE, a cluster containing 70 targets was constructed. The cluster was further assessed with cytoHubba, and the top-10 targets were selected according to their degree values; these included MAPK1, MAPK3, JUN, IL6, AKT1, TNF, PTGS2, MMP9, STAT3 and CXCL8 (Figure 4).

GO and KEGG Pathway Enrichment Analysis

GO analysis of the 276 common targets using the DAVID system revealed that the functions of these potential targets were related to many biological processes, molecular functions, and cellular components (Figure 5).

Based on the *P* value, the top 20 significantly enriched KEGG pathways for the 276 common targets was identified to decipher the putative mechanism underlying the effect of ASSD on RA. As shown in Figure 6, inflammation-related pathways, such as the PI3K-AKT, TNF-, and IL-17 signaling pathways, were involved in ASSD-mediated RA treatment.

https://doi.org/10.2147/DDDT.S489323

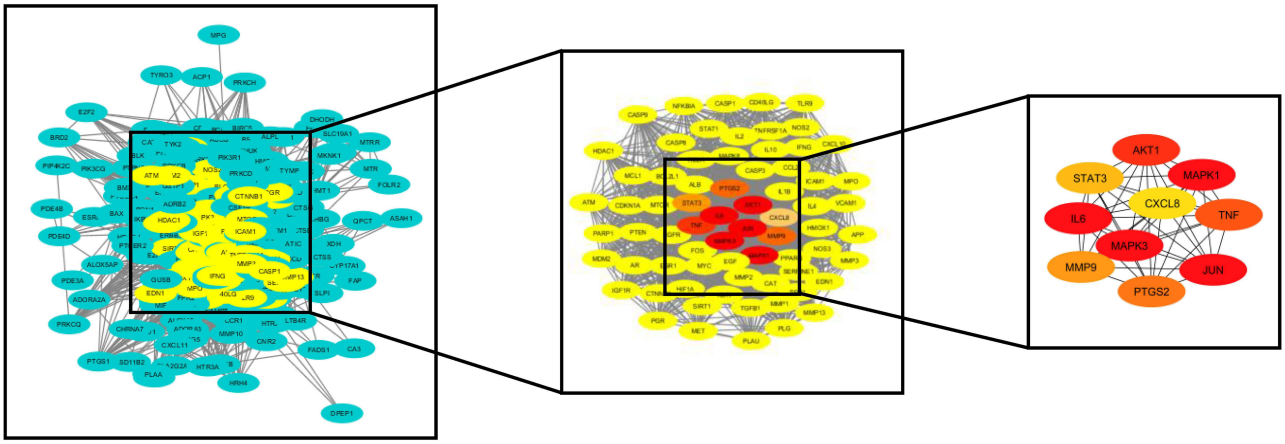

Figure 4 Protein–protein interaction (PPI) network of the 276 potential targets. The nodes represent proteins, and edges represent protein–protein interactions.

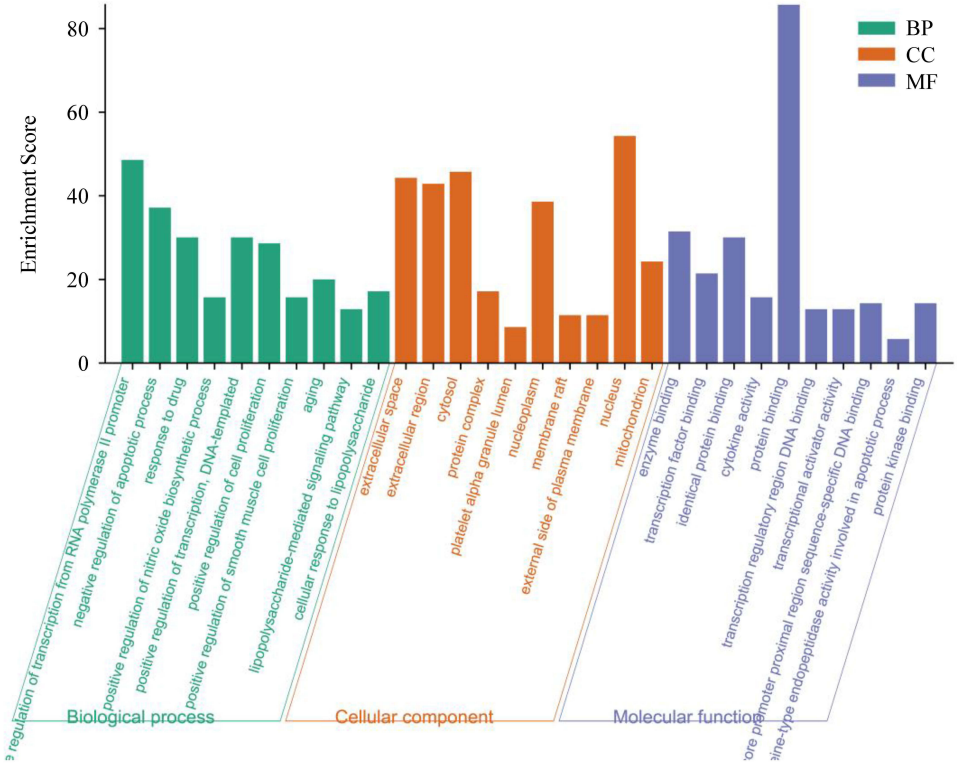

Figure 5 Gene ontology (GO) enrichment with the top-10 *P*-values for each item.

Kaempferol, Luteolin, and Quercetin Inhibited LPS+IFN-γ-Induced Inflammatory Responses in RAW 264.7 cells

Using the network and pathway analyses, kaempferol, luteolin, and quercetin were found to be the key ingredients of ASSD responsible for its effect against RA. The anti-inflammatory properties of these ingredients could provide the major mechanism for ASSD-mediated RA treatment. Therefore, the anti-inflammatory effects of kaempferol, luteolin, and quercetin were investigated in LPS-induced RAW 264.7 cells.

The cytotoxicity of kaempferol, luteolin, and quercetin was evaluated by treating the RAW 264.7 cells with various concentrations of these compounds for 24 h using the CCK-8 assay. Kaempferol, luteolin, and quercetin did not affect the

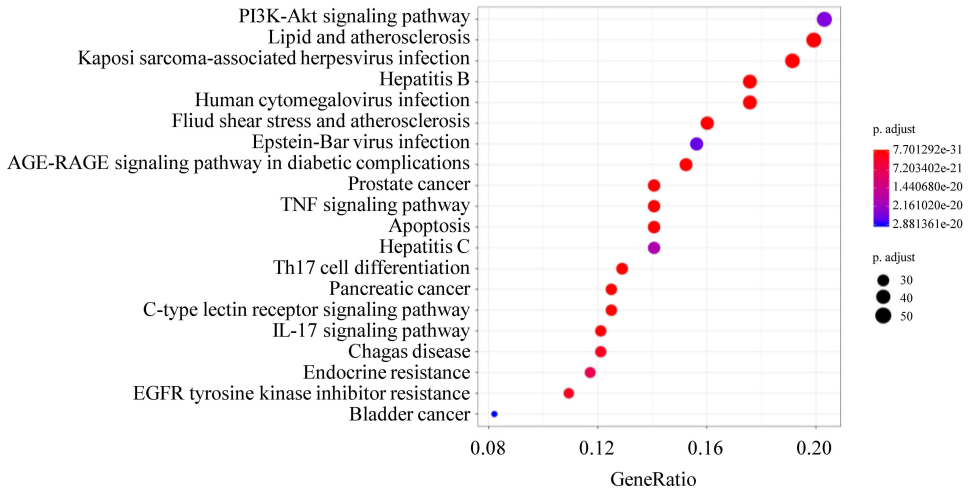

Figure 6 Kyoto encyclopedia of genes and genomes (KEGG) enrichment with the top-20 *P*-values.

viability of RAW 264.7 cells at concentrations of 60, 40, and 60 μmol/L, respectively (Figure 7a). Therefore, concentrations between 1 and 40 μmol/L were selected for subsequent experiments.

NO is a key factor promoting the development of inflammatory responses. The production of NO in LPS+IFN-γ-treated cells was markedly increased, as measured using the Griess reagent; however, treatment with kaempferol, luteolin, and quercetin alleviated the LPS+IFN-γ-induced increase in NO levels in a concentration-dependent manner (Figure 7b).

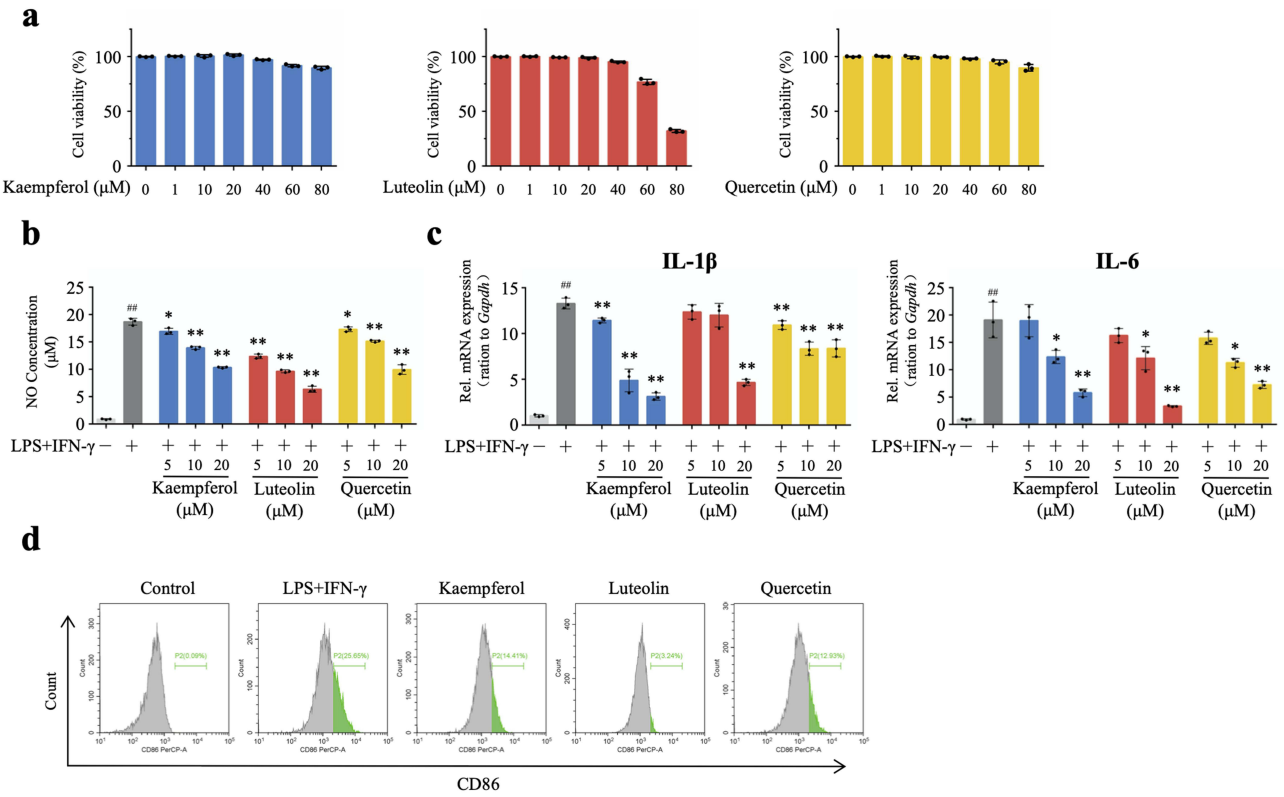

Figure 7 Inhibition of lipopolysaccharide (LPS)+interferon gamma (IFN-γ)-induced inflammatory responses in RAW 264.7 cells by kaempferol, luteolin, and quercetin. (**a**) Cytotoxicity of kaempferol, luteolin, and quercetin in RAW 264.7 cells after 24 h of treatment. (**b**) Nitric oxide (NO) levels in the culture medium were measured using the Griess reagent. (**c**) Quantitative RT-PCR analysis of the mRNA levels of *Il1b* and *Il6* in RAW 264.7 cells stimulated with LPS+IFN-γ in the presence of the indicated doses of kaempferol, luteolin, or quercetin for 24 h. (**d**) Flow cytometry analysis of Cd86 expression in RAW 264.7 cells stimulated with LPS+IFN-γ in the presence of kaempferol, luteolin, or quercetin (20 μmol/L) for 24 h. Three samples were analyzed for each group. The data were analyzed using an unpaired *t*-test. ## *P*<0.01 compared with the control group, * *P*<0.05 and ** *P*<0.01 compared with the LPS+IFN-γ group. Bar graphs show mean ± SD.

https://doi.org/10.2147/DDDT.S489323

To further explore the anti-inflammatory effects of kaempferol, luteolin, and quercetin, the mRNA levels of inflammatory factors were measured using RT-PCR. LPS+IFN-γ stimulated the production of proinflammatory cytokines, including Il1b and Il6, which was significantly reduced by treatment with kaempferol, luteolin, and quercetin (Figure 7c). Moreover, kaempferol, luteolin, and quercetin decreased the levels of LPS+IFN-γ-simulated proinflammatory cytokines in a dose-dependent manner.

Under the action of LPS+IFN-γ, macrophages manifest the classically activated phenotype (M1). To confirm the effect of kaempferol, luteolin, and quercetin on M1 macrophages, the expression of M1 marker Cd86 was analyzed using flow cytometry. Kaempferol, luteolin, and quercetin treatment led to a significantly lower percentage of M1 macrophages thanLPS+IFN-γ stimulation (Figure 7d).

Inhibition of Glycolysis Involves Kaempferol, Luteolin, and Quercetin-Mediated Anti-inflammatory Responses

Because mitochondrial ROS production is central to determining the inflammatory phenotype of macrophages,[19] we examined the effects of kaempferol, luteolin, and quercetin on mitochondrial ROS levels using MitoSOX. Addition of LPS+IFN-γ led to an increase in mitochondrial ROS levels, which were decreased by kaempferol, luteolin, and quercetin in a dose-dependent manner (Figure 8a). Following LPS stimulation, macrophages repurpose their mitochondria from ATP production to ROS generation, with glycolysis taking on the role of ATP generation to promote a proinflammatory phenotype.[19] To examine the roles of kaempferol, luteolin, and quercetin in glycolysis, we performed RNA sequencing. Genes involved in glycolysis were upregulated by LPS+IFN-γ, but they were downregulated by kaempferol, luteolin, and quercetin, suggesting that glycolysis is crucial for the kaempferol-, luteolin-, and quercetin-mediated anti-inflammatory action (Figure 8b–d).

The LPS+IFN-γ treatment also decreased the ATP/ADP ratio, which is consistent with the shift in ATP synthesis from oxidative phosphorylation to glycolysis; however, kaempferol, luteolin, and quercetin restored the ATP/ADP ratio (Figure 8e). The NAD^+/NADH ratio was also decreased upon LPS+IFN-γ treatment as the conversion of pyruvate to lactate in glycolysis regenerates cytosolic oxidized NAD^+ to support glycolytic ATP generation, which was enhanced in the presence of kaempferol, luteolin, and quercetin (Figure 8f). Taken together, these results indicate that kaempferol, luteolin, and quercetin prevent the expression of proinflammatory factors via the inhibition of glycolysis.

Kaempferol, Luteolin, and Quercetin Suppress Glycolysis Through PI3K-AKT Signaling

Macrophages upregulate the glycolytic module, which is linked to excess glucose uptake and increased expression of the glucose transporter, Glut1.[20,21] Consistent with previous reports, LPS+IFN-γ induced a time-dependent increase in the expression of Glut1 (Figure 9a). Kaempferol, luteolin, and quercetin treatment not only decreased the expression of Glut1 (Figure 9b), but also reduced glucose consumption (Figure 9c).

Lactate dehydrogenase A (Ldha) is a glycolytic enzyme that converts pyruvate to lactate and is induced under intensified glycolysis.[22] Immunoblot analysis revealed that activation of macrophages with LPS+IFN-γ enhanced the expression of Ldha in a time-dependent manner, in consonance with the induction of the Ldha transcriptional regulator, c-Myc (Figure 9d). Treatment with kaempferol, luteolin, or quercetin significantly reduced the expression of Ldha and c-Myc (Figure 9e).

Glut 1 and Ldha are induced in $CD8^+$ T effector cells via PI3K-AKT signaling.[22] In macrophages, upon LPS+IFN-γ stimulation with increasing time, PI3K-dependent Akt phosphorylation showed a response curve similar to that of Ldha and c-Myc (Figure 9f). To investigate whether PI3K-AKT signaling was involved in the expression of Glut 1 and Ldha, a PI3K-specific inhibitor, CAL-101, was used (Figure 9g). The blockade of PI3K signaling with increasing doses of CAL-101 progressively repressed the expression levels of Glut1, Ldha, and c-Myc (Figure 9h). To further determine the role of PI3K-AKT signaling in kaempferol-, luteolin-, and quercetin-mediated inhibition of glycolysis, we examined Akt phosphorylation and found that it was decreased by kaempferol, luteolin, and quercetin treatments (Figure 9i). Taken together, these data suggest that kaempferol, luteolin, and quercetin act through the PI3K-AKT pathway to decrease the expression of Glut1 and Ldha, thereby inhibiting glycolysis.

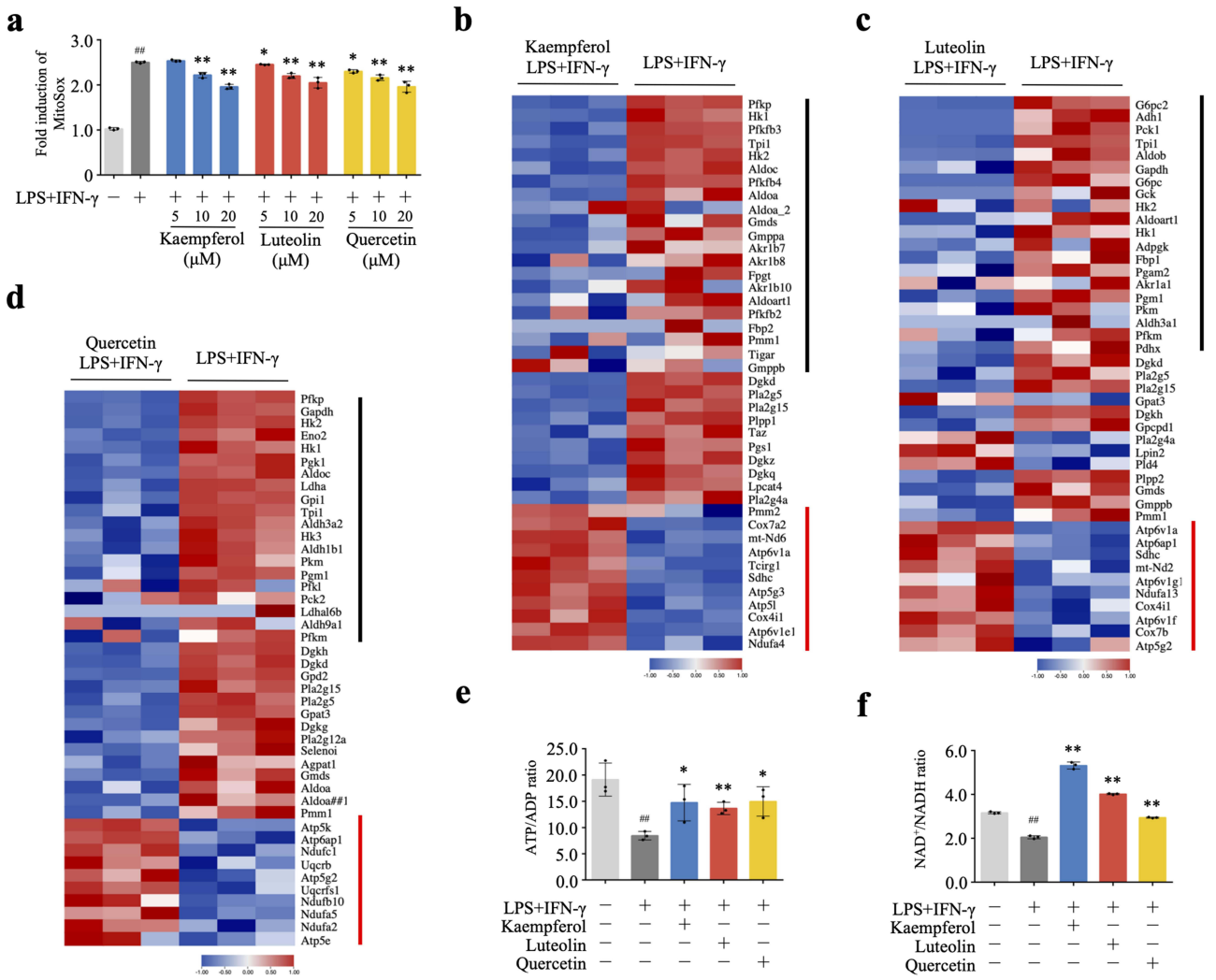

Figure 8 Inhibition of glycolysis involves kaempferol, luteolin, and quercetin-mediated anti-inflammatory responses. (**a**) MitoSox staining, indicative of mitochondrial ROS levels, of RAW 264.7 cells stimulated with lipopolysaccharide (LPS)+ interferon gamma (IFN-γ) in the presence of the indicated doses of kaempferol, luteolin, or quercetin for 24 h. (**b-d**) Heat map of statistically differentially expressed genes by RNA sequencing transcriptome analysis in RAW 264.7 cells stimulated with LPS+IFN-γ in the presence of kaempferol, luteolin, or quercetin (20 μmol/L) for 24 h. Black Bar points to the genes downregulated in glycolysis and red bar points to the genes upregulated in oxidative phosphorylation. (**e**) The ATP/ADP ratio in cell lysates was determined using an ATP/ADP assay kit. (**f**) The NAD^+/NADH ratio in cell lysates was determined using an NAD^+/NADH assay kit. Three samples were analyzed for each group. The data were analyzed using an unpaired *t*-test. $^{\#\#}$ *P*<0.01 compared with the control group, * *P*<0.05 and ** *P*<0.01 compared with the LPS+INF-γ group. Bar graphs show mean ± SD.

Molecular Docking and Molecular Dynamics Simulation

Kaempferol, luteolin, and quercetin exhibited the same inhibitory effect on AKT phosphorylation as CAL101, which is a potent and selective ATP-competitive inhibitor of PI3Kδ. Molecular docking revealed that kaempferol, luteolin, and quercetin occupied the cleft formed between the N- and C-lobes of the kinase domain of PI3Kδ, which is the hydrophobic pocket for ATP binding (Figure 10a–c). The hydrogen bond, hydrophobic interaction, and van der Waals (VDW) force are the main forces that maintain interactions between PI3Kδ and the compounds.

To further evaluate the structural stability of PI3Kδ and compounds, molecular dynamics simulation was performed. Root mean square deviation (RMSD) is an essential factor to evaluate the stability of a system. The RMSD of the complex structures, proteins, and compounds gradually stabilized as the simulation progressed, without significant fluctuations, indicating that the complex structure gradually stabilized (Figure 11a). Centroid evolution analysis was performed by measuring the distance between the initial binding site and compounds and the distance between the protein center and compounds to evaluate the binding state. Figure 11b shows that the distance between the initial binding site and compounds fluctuated slightly, and the distance between the protein center and compounds was stable,

https://doi.org/10.2147/DDDT.S489323

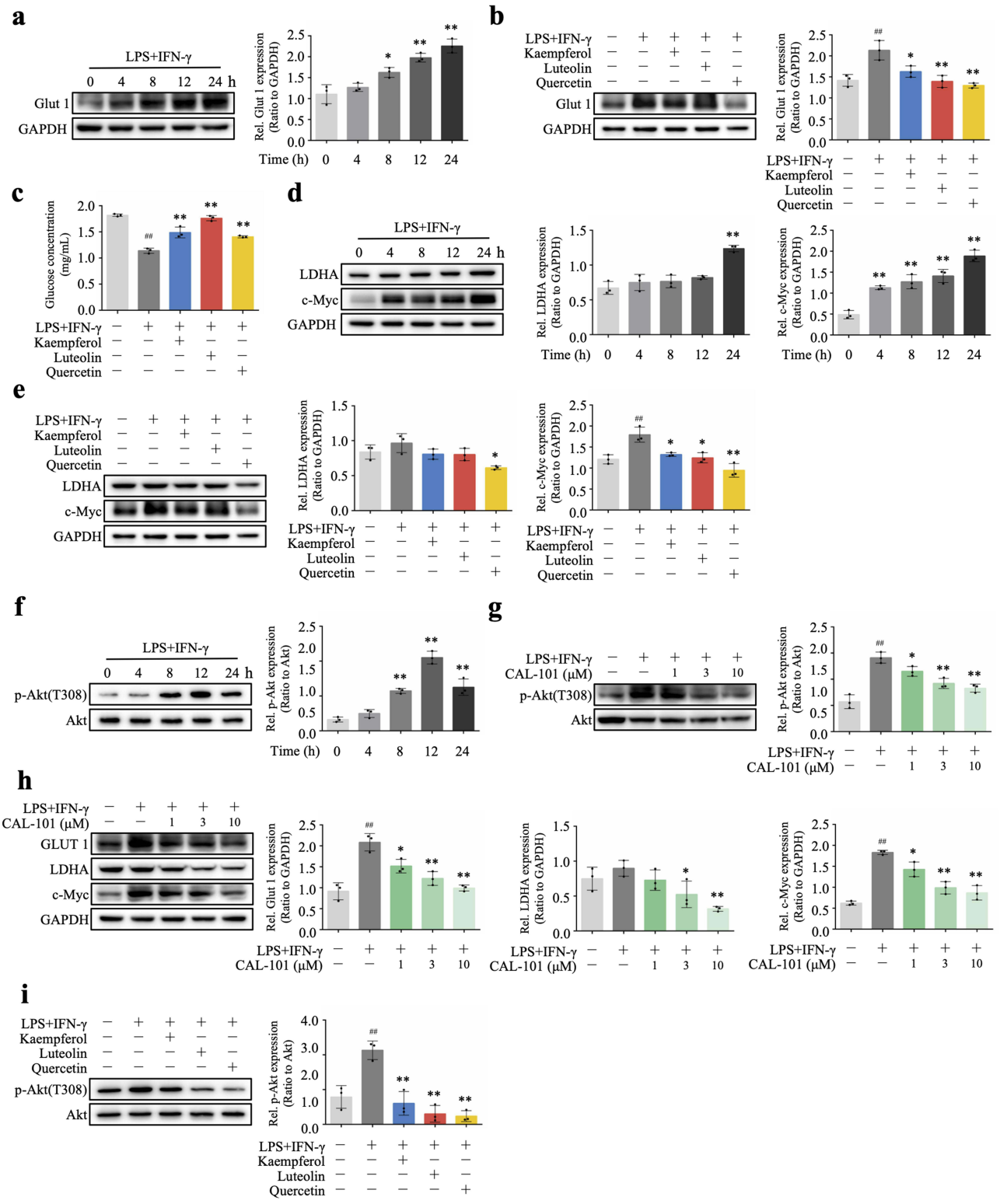

Figure 9 Kaempferol, luteolin, and quercetin suppressed glycolysis through the PI3K-AKT signaling. (**a-d**) RAW 264.7 cells were stimulated with lipopolysaccharide (LPS)+ interferon gamma (IFN-γ) for the indicated time points. Immunoblotting and normalized expression of Glut, Ldha, and c-Myc against GAPDH. (**b-e**) RAW 264.7 cells were stimulated with LPS +IFN-γ in the presence of kaempferol, luteolin, or quercetin (20 μmol/L) for 24 h. Immunoblotting and normalized expression of Glut, Ldha, and c-Myc against GAPDH. (**c**) Glucose levels in the culture medium were measured with a glucose assay kit. (**f**) RAW 264.7 cells were stimulated with LPS+IFN-γ for the indicated time points. Immunoblotting and normalized expression of p-Akt (T308) against Akt. (**g** and **h**) RAW 264.7 cells were stimulated with LPS+IFN-γ in the presence of the PI3K inhibitor CAL-101 (1, 3, or 10 μmol/L) for 24 h. The immunoblot shows normalized expression of p-Akt (T308) against Akt as well as of Glut, Ldha, and c-Myc against GAPDH. (**i**) RAW 264.7 cells were stimulated with LPS+IFN-γ in the presence of kaempferol, luteolin, or quercetin (20 μmol/L) for 24 h. Immunoblotting and normalized expression of p-Akt (T308) against Akt. Three samples were analyzed for each group. The data were analyzed using an unpaired *t*-test. $^{\#\#}$ $P<0.01$ compared with the control group, * $P<0.05$ and ** $P<0.01$ compared with the LPS+IFN-γ group. Bar graphs show mean ± SD.

https://doi.org/10.2147/DDDT.S489323

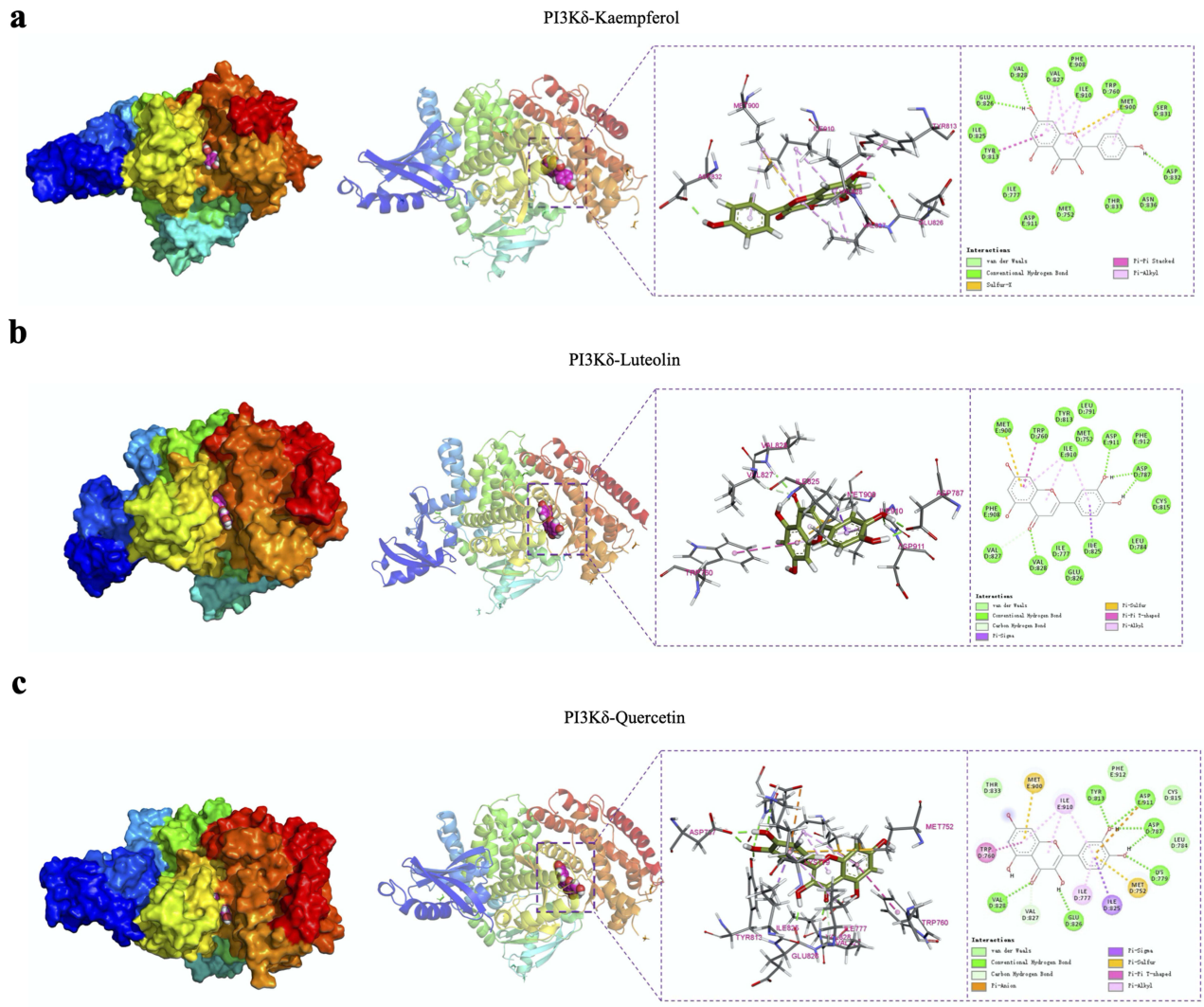

Figure 10 Molecular docking of PI3kδ and the compounds. (**a**) Binding mode of PI3kδ and kaempferol. (**b**) Binding mode of PI3kδ and luteolin. (**c**) Binding mode of PI3kδ and quercetin.

indicating that compounds did not deviate from and stably bound the initial binding site and the protein center. Buried SASA evaluated the binding state by measuring the size of the binding interface between the protein and compound. Figure 11c showed that the embedding areas of kaempferol, luteolin, and quercetin in the protein of the complex were stable with slight fluctuations, indicating that the binding interface between PI3Kδ and the compounds was stable The high degree of simulated conformational overlap indicates that small molecules always bind to the initial site. Figure 11d shows that the superimposed conformation of the compounds in the complex was near the initial binding site, and the degree of conformation overlap was strong, indicating that compounds bound to the initial binding site of the protein during the simulation.

Hydrogen bonding is an important interaction force between proteins and ligands, which can reflect the strength of electrostatic interactions. During the simulation, the number of hydrogen bonds for kaempferol, luteolin, and quercetin mainly fluctuated between 2 and 3, 3 and 4, and 4 and 6, respectively (Figure 12a). To further identify the residues that form hydrogen bonds with compounds in the protein and the stability of hydrogen bonds, the percentage of hydrogen bonds formed between PI3Kδ and the compounds was analyzed. During the simulation, the hydrogen bonds, 828VAL: ligand (Figure 12b), 828VAL:ligand (Figure 12c), 813TYR:ligand (Figure 12d), 828VAL:ligand (Figure 12d) and ligand:826GLU (Figure 12d), were formed with high frequency, high occupancy, and strong stability.

https://doi.org/10.2147/DDDT.S489323

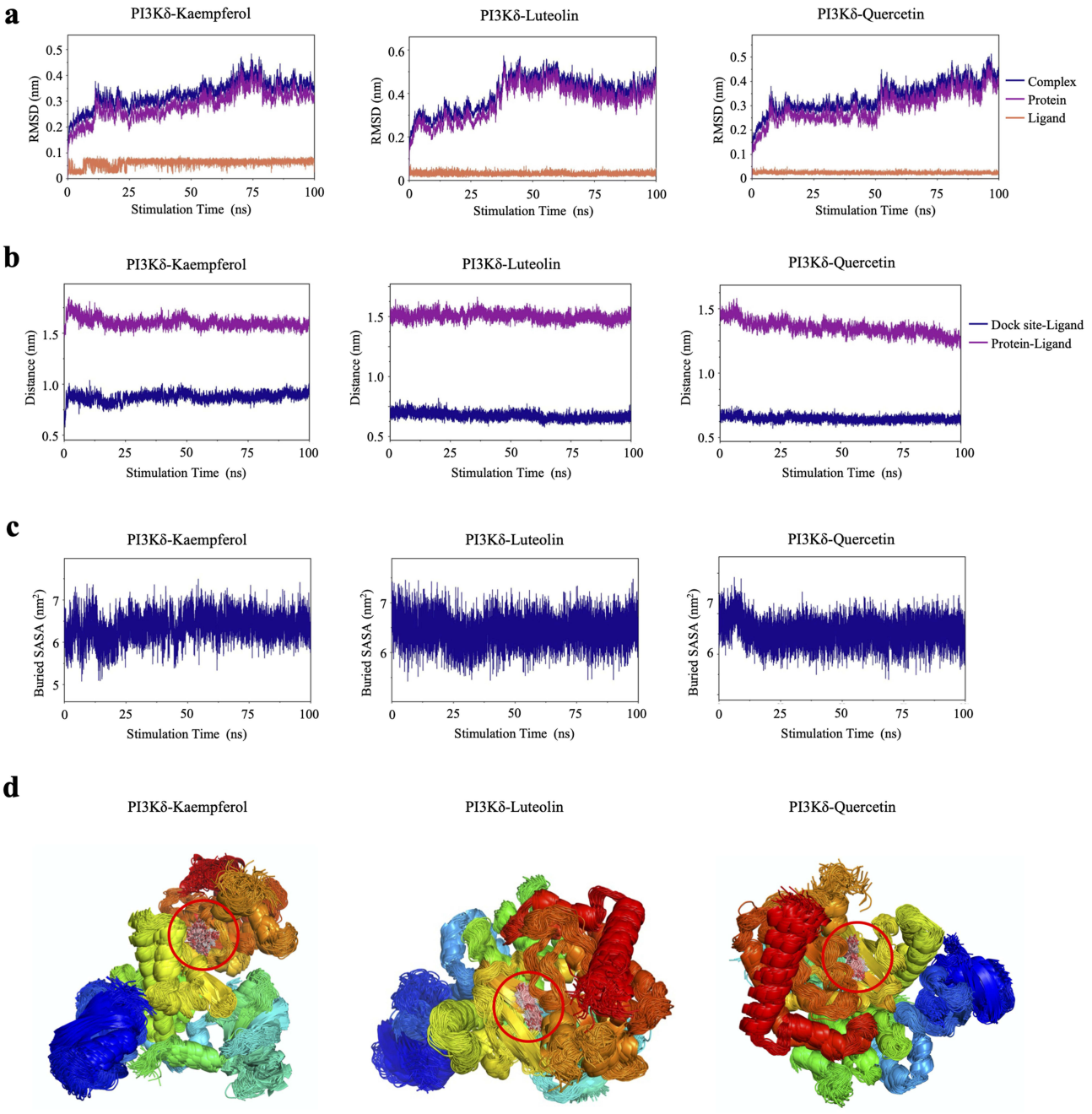

Figure 11 Stability analysis of PI3kδ and compounds in molecular dynamic simulations. (**a**) RMSD of the protein, ligand, and protein-ligand complex. (**b**) Centroid evolution analysis of PI3kδ and compounds. (**c**) Buried SASA analysis of PI3kδ and compounds. (**d**) The simulated conformational congruence of PI3kδ and the compounds.

The VDW and electrostatic (ELE) interaction forces between PI3Kδ and the compounds were calculated without considering solvation, and the binding forces were analyzed during the simulation. The ELE interaction fluctuated considerably compared with the VAW forces, but the ELE interaction gradually stabilized, indicating that the binding between PI3Kδ and the compounds was stable (Figure 13a). The binding energies between PI3Kδ and kaempferol, luteolin, and quercetin were −72.364 ± 2.505, −61.419 ± 0.801, and −64.034 ± 2.839 kJ/mol, respectively, with considering solvation (Table 1). The binding energy was decomposed to obtain the contribution of each amino acid to the overall binding energy. Figure 13b shows that the key amino acids in the PI3Kδ-kaempferol, PI3Kδ-luteolin, and PI3Kδ-quercetin complexes were ILE-910, MET-900, and ILE-825, respectively.

 https://doi.org/10.2147/DDDT.S489323

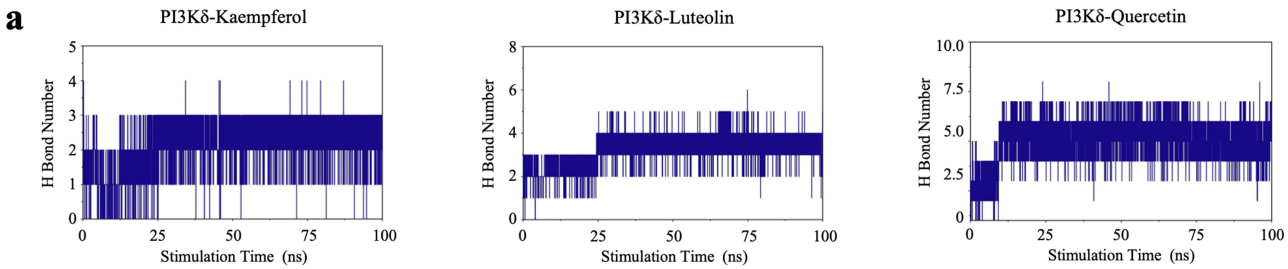

b

PI3Kδ-Kaempferol

Index	Dornor	Acceptor	Occupancy
1	828VAL (chain D#N)	Ligand (11539#O)	82.8%
2	Ligand (11536#O)	832ASP (chain D#OD1)	72.1%
3	Ligand (11537#O)	911ASP (chain E#OD1)	2.9%
4	Ligand (11537#O)	911ASP (chain E#OD2)	2.6%
5	Ligand (11539#O)	826GLU (chain D#O)	66.8%

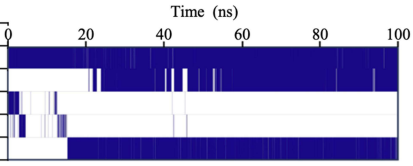

c

PI3Kδ-Luteolin

Index	Dornor	Acceptor	Occupancy
1	779LYS (chain D#NZ)	Ligand (11537#O)	3.8%
2	828VAL (chain D#N)	Ligand (11535#O)	97.0%
3	911ASP (chain E#N)	Ligand (11536#O)	35.6%
4	912PHE (chain E#N)	Ligand (11536#O)	1.9%
5	Ligand (11536#O)	787ASP (chain D#OD2)	72.9%
6	Ligand (11536#O)	813TYR (chain D#OH)	26.1%
7	Ligand (11537#O)	787ASP (chain D#OD2)	73.9%

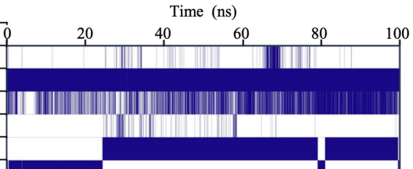

d

PI3Kδ-Quercetin

Index	Dornor	Acceptor	Occupancy
1	779LYS (chain D#NZ)	Ligand (11537#O)	18.8%
2	813TYR (chain D#OH)	Ligand (11535#O)	94.8%
3	828VAL (chain D#N)	Ligand (11536#O)	96.9%
4	911ASP (chain E#N)	Ligand (11536#O)	27.0%
5	Ligand (11536#O)	787ASP (chain D#OD1)	57.5%
6	Ligand (11536#O)	787ASP (chain D#OD2)	33.1%
7	Ligand (11537#O)	787ASP (chain D#OD1)	57.4%
8	Ligand (11537#O)	787ASP (chain D#OD2)	33.0%
9	Ligand (11538#O)	826GLU (chain D#O)	83.9%

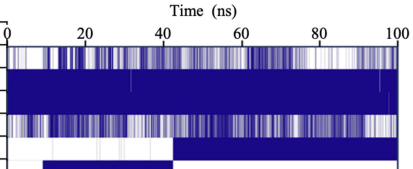

Figure 12 Analysis of hydrogen bond interaction of PI3kδ and compounds in molecular dynamic simulations. (**a**) Hydrogen bond map of PI3kδ and compounds. (**b**) The occupancy of hydrogen bonds for PI3kδ and kaempferol. (**c**) The occupancy of hydrogen bonds for PI3kδ and luteolin. (**d**) The occupancy of hydrogen bonds for PI3kδ and quercetin.

PI3Kδ Was Elevated in Synovial Tissue of RA Patients

To identify the role of PI3Kδ in RA, PI3Kδ expression in the synovial tissue of patients with RA was profiled by bioinformatics analysis of two publicly available GSE datasets. In the GSE55235 dataset, the mRNA of PI3Kδ (gene name is PIK3CD) was significantly upregulated in the synovial tissue of patients with RA (n = 10) compared with those in the synovial tissue of healthy people (n = 10) (Figure 14a). PI3Kδ was also highly expressed in the GSE55457 dataset (n = 10 for health controls and n = 13 for RA) (Figure 14a). Interleukin 7 (Il7), interleukin 15 (Il15), and interleukin 18 (Il18) were considered key biomarkers in RA development and progression that act as mediators in the etiology of RA and also serve as a diagnostic tool for RA. Specifically, the levels of PI3Kδ showed a positive correlation with the levels of Il7, Il15, and Il18 in the synovial tissue of patients with RA (Figure 14b–d). This shows that PI3Kδ plays the role of a promoter in RA and PI3Kδ may be potentially targeted to treat RA.

Discussion

In this study, network pharmacology analysis of the 75 active ingredients of ASSD and the 1258 RA-related targets revealed that kaempferol, luteolin, and quercetin are the key ingredients of ASSD, and MAPK1, MAPK3, JUN, IL6,

https://doi.org/10.2147/DDDT.S489323

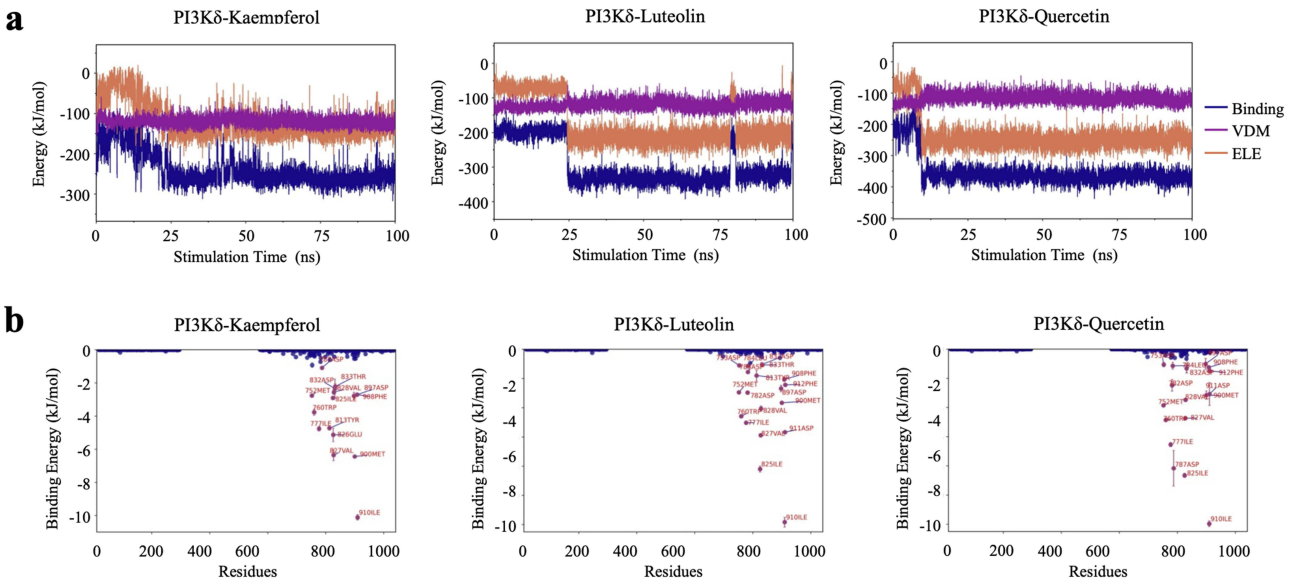

Figure 13 Analysis of the interaction and key amino acid residues of PI3kδ and the compounds in molecular dynamic simulations. (**a**) van der Waals force (VDW) and electrostatic (ELE) interaction analysis of PI3kδ and compounds. (**b**) The key amino acid residues between PI3kδ and compounds.

AKT1, TNF, PTGS2, MMP9, STAT3, and CXCL8 are the key targets of ASSD for RA treatment. The inflammatory-related pathways (the PI3K-AKT, TNF, and IL17 signaling pathways) were predicted to be involved in ASSD-mediated RA treatment. With the goal of ensuring low disease activity or remission, a tight control of inflammation is the central focus of the pharmacological treatment of RA.

TNF and IL6 are the underlying targets of ASSD-mediated protection against RA. The critical roles of TNF and IL6 in RA are strongly supported by the successful clinical benefits of anti-TNF and anti-IL6 therapies.[2] In RA, TNF is mainly produced by monocytes and macrophages and also by T cells, B cells, and synovial fibroblasts.[23,24] TNF primes for or directly mediates leukocyte and endothelial cell activation, adhesion, and migration, synovial fibroblast activation and survival, cytokine release, and angiogenesis, which together represent key pathological features of RA.[23] Patients with RA who exhibit inadequate response to csDMARD often have to receive a first line TNF-α inhibitor as the initial bDMARD, unless contraindicated.[1] Approximately 70% of patients with RA respond to therapeutic inhibition of TNF with antibodies or soluble receptors.[23] In RA, IL6 is mainly produced by monocytes, synovial fibroblasts, B cells, and T cells.[23] IL6 regulates innate responses similar to TNF in the local synovial environment, but it also directly drives the acute-phase response.[25,26] In addition, IL6 performs an essential immunoregulatory role in adaptive immunity, participating in the differentiation of naïve T-cell toward the proinflammatory T_H 17 cell or regulatory T_{REG} cell pathway.[25] Targeting IL6 with neutralizing antibodies or Janus kinase (JAK) inhibitors has been shown to be effective against RA.[27] However, there may be some degree of specificity in eliciting inflammatory subgroups and synovial changes between TNF and IL6 inhibition.[25,28] Reduction in TNF and IL6 levels is indeed involved in the treatment of RA with *A. membranaceus*,[29] *L. japonica*,[30] *P. cuspidatum*,[31] and *H. diffusa*,[32] which is consistent with the prediction that the therapeutic effects of ASSD against RA are mediated, at least in part, via TNF and IL6.

Table 1 Binding Free Energy of PI3Kδ with the Compounds (kJ/Mol)

Complex	ΔE_{VDW}	ΔE_{ele}	ΔE_{pol}	ΔE_{nonpol}	ΔG_{bind}
PI3Kδ-Kaempferol	−139.4±0.925	−63.467±0.988	147.813±1.713	−17.311±0.113	−72.364±2.505
PI3Kδ-Luteolin	−127.289±2.323	−97.512±4.671	180.68±1.847	−17.298±0.054	−61.419±0.801
PI3Kδ-Quercetin	−139.114±4.5	−125.144±3.341	217.266±3.974	−17.042±0.111	−64.034±2.839

Note: ΔE_{vdw} van der Waals energy; ΔE_{ele}, electrostatic energy; ΔE_{pol}, polar solvation energy; ΔE_{nonpol}, nonpolar solvation energy; ΔG_{bind}, binding free energy. $\Delta G_{bind} = \Delta E_{vdw} + \Delta E_{ele} + \Delta E_{pol} + \Delta E_{nonpol}$.

https://doi.org/10.2147/DDDT.S489323

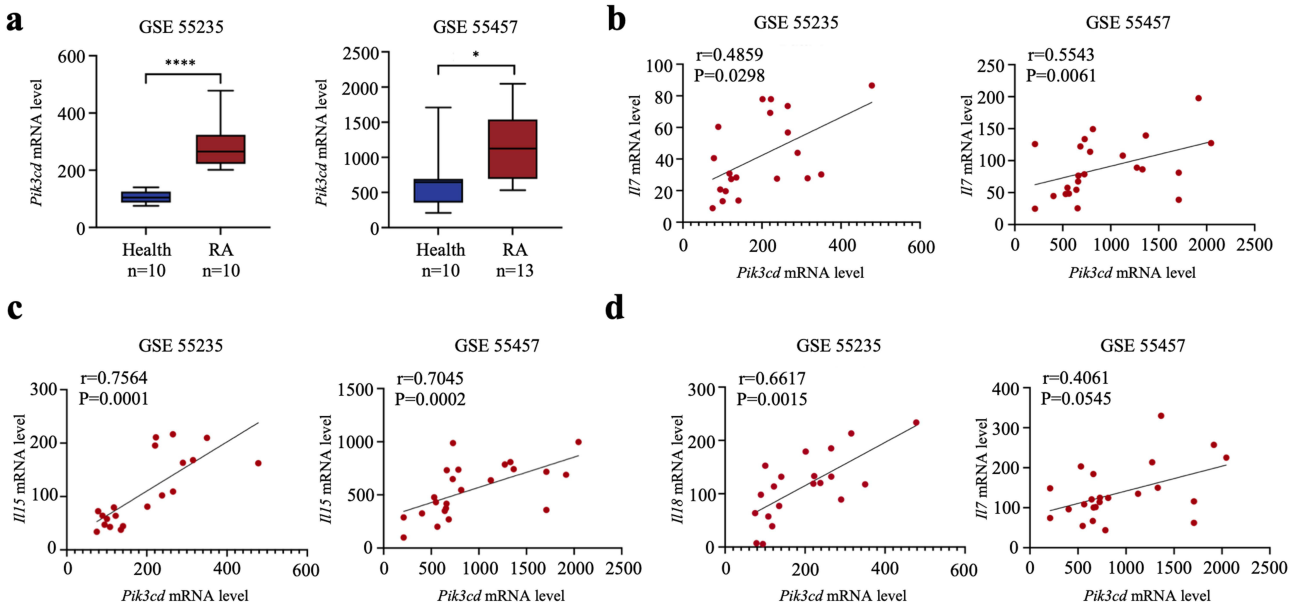

Figure 14 PI3kδ was elevated in the synovial tissue of patients with RA. (**a**) The mRNA levels of *Pik3cd* (gene name of PI3kδ) in synovial specimens of RA in the GSE55235 and GSE55457 datasets. Unpaired *t*-test. * $P<0.05$ and **** $P<0.0001$ compared with the healthy group. (**b-d**) Pearson's correlation of *Pik3cd* with the mRNA levels of Il7, Il15, and Il18 in RA in the GSE55235 and GSE55457 datasets. Two-tailed Pearson χ^2 test.

The PI3K-AKT signaling pathway is assumed to play a crucial role in the antirheumatic effects of ASSD. PI3Ks are a large family of lipid kinases that phosphorylate phosphoinositides and are divided into classes I, II, and III. Class I PI3Ks are further divided into class IA (comprising the PI3Kα, PI3Kβ, and PI3Kδ isoforms) and class IB (comprising PI3Kγ only), among which PI3Kδ and PI3Kγ are mainly expressed in leukocytes.[33] AKT, a serine/threonine kinase, is the central mediator of PI3Ks and has multiple downstream effectors.[34] The PI3K-AKT signaling pathway, most notably mediated by PI3Kδ and PI3Kγ, participates in multiple steps and various stages of RA pathogenesis, such as in antigen signaling in B and T cells, signaling downstream of FcRs, and cytokine receptors and chemokine receptors in mast cells, macrophages, neutrophils, and synoviocytes.[33] In vivo and in vitro studies have shown that inhibition of the PI3K-AKT signaling pathway through pharmacological inhibitors or genetic deletion of PI3Ks can reduce inflammatory cell infiltration, synoviocyte proliferation and survival, and bone destruction in RA.[34–37] The PI3K-AKT signaling pathway has attracted considerable research interest as a pharmacological target in the treatment of RA. Based on the wide range of PI3K-AKT signaling in RA, ASSD may have specific roles at all stages of RA progression via this signaling pathway.

According to the results of network and pathway analyses, kaempferol, luteolin, and quercetin are the key ingredients of ASSD involved in its effect against RA, and the anti-inflammatory effect is the major mechanism underlying ASSD-mediated RA treatment. Thus, the role of kaempferol, luteolin, and quercetin in the anti-inflammatory effects was explored in LPS-stimulated RAW 264.7, and it was found that all three ingredients decreased the production of proinflammatory factors in macrophages. The inhibition of glycolysis plays a crucial role in the anti-inflammatory properties of kaempferol, luteolin, and quercetin. The anti-inflammatory effects of kaempferol, luteolin, and quercetin have been reported previously;[38–40] however, investigations on the pharmacological mechanism have mainly focused on signaling pathways, such as NF-κB, MAPK, and JAK/STAT, but not on glycolysis. Upon LPS stimulation, macrophages shift from ATP production via oxidative phosphorylation to glycolysis.[19] Glycolysis is less efficient than aerobic oxidation, but may prepare macrophages for the rapid activation and synthesis of immune mediators required to perpetuate inflammation; thus, it is used by inflammatory macrophages.[41,42] In this study, the inhibition of PI3K-AKT signaling by kaempferol, luteolin, and quercetin decreased the glucose uptake and pyruvate-to-lactate conversion by diminishing the expression of Glut1 and Ldha, which inhibits glycolytic metabolism. PI3K-AKT signaling plays a multifaceted role in controlling glucose metabolism in T effector cells by promoting the expression of Glut1 and LDHA.[22] We found that glycolysis in macrophages was also controlled by PI3K-AKT signaling via a similar mechanism.

https://doi.org/10.2147/DDDT.S489323

In the inflamed joints, glucose and lactate concentrations were distinctly low and high, respectively. Moreover, macrophages from patients with RA commit to a hypermetabolic state with intensified glycolysis.[43] Future studies are required to investigate the role of ASSD in glycolysis, inflammation, and disease activity in animal models of RA. Targeting metabolic checkpoints may provide new opportunities for developing alternative RA treatment strategies.

Conclusion

In conclusion, using integrated network pharmacology, we identified kaempferol, luteolin, and quercetin as the key components of ASSD that can be used to treat RA via inhibition of inflammation. We further confirmed that kaempferol, luteolin, and quercetin inhibited LPS-induced glycolysis in macrophages by blocking PI3K-AKT signaling, leading to a decreased expression of proinflammatory factors. Kaempferol, luteolin, and quercetin stably occupied the hydrophobic pocket of PI3Kδ, which may be the potential target of kaempferol, luteolin, and quercetin to treat RA. The various active ingredients of ASSD lead to synergistic effects on RA by acting on multiple targets and pathways. The findings of this study only partly reveal the complex effect of ASSD in RA but can provide new directions that would improve the overall understanding underlying the therapeutic value of this decoction.

Data Sharing Statement

The datasets supporting the conclusions of this article are included within the article. Further inquiries can be addressed to the corresponding author.

Ethics Approval and Consent to Participate

This study is involving human data from public datasets Genecards, TTD and GEO. The Ethics Committee of Shanxi University of Chinese Medicine has approved this study.

Acknowledgments

We want to thank for academic and technical assistances of the Shanxi Leader Team of Medical Science & Technology Innovations (Grant: 2020TD02). The Leader Team contributes to the manuscript but does not qualify for authorship.

Funding

This work was supported by Natural Science Foundation of Shanxi Province (201801D221437).

Disclosure

The authors have declared no conflicts of interest in this work.

References

1. Sparks JA. Rheumatoid Arthritis. *Ann Intern Med*. 2019;170:Itc1–itc16. doi:10.7326/AITC201901010
2. Aletaha D, Smolen JS. Diagnosis and Management of Rheumatoid Arthritis: a Review. *JAMA*. 2018;320:1360–1372. doi:10.1001/jama.2018.13103
3. Weyand CM, Goronzy JJ. The immunology of rheumatoid arthritis. *Nat Immunol*. 2021;22:10–18. doi:10.1038/s41590-020-00816-x
4. Janossy G, Panayi G, Duke O, et al. Rheumatoid arthritis: a disease of T-lymphocyte/macrophage immunoregulation. *Lancet*. 1981;2:839–842.
5. Udalova IA, Mantovani A, Feldmann M. Macrophage heterogeneity in the context of rheumatoid arthritis, Nature reviews. *Rheumatology*. 2016;12:472–485. doi:10.1038/nrrheum.2016.91
6. Hamilton JA, Tak PP. The dynamics of macrophage lineage populations in inflammatory and autoimmune diseases. *Arthritis Rheum*. 2009;60:1210–1221. doi:10.1002/art.24505
7. Boutet MA, Courties G, Nerviani A, et al. Novel insights into macrophage diversity in rheumatoid arthritis synovium. *Autoimmun Rev*. 2021;20:102758. doi:10.1016/j.autrev.2021.102758
8. Haringman JJ, Gerlag DM, Zwinderman AH, et al. Synovial tissue macrophages: a sensitive biomarker for response to treatment in patients with rheumatoid arthritis. *Ann Rheum Dis*. 2005;64:834–838. doi:10.1136/ard.2004.029751
9. Nerviani A, Di Cicco M, Mahto A, et al. A Pauci-Immune Synovial Pathotype Predicts Inadequate Response to TNFα-Blockade in Rheumatoid Arthritis Patients. *Front Immunol*. 2020;11:845. doi:10.3389/fimmu.2020.00845
10. Ru J, Li P, Wang J, et al. TCMSP: a database of systems pharmacology for drug discovery from herbal medicines. *J Cheminf*. 2014;6:13. doi:10.1186/1758-2946-6-13
11. Liu Z, Guo F, Wang Y, et al. BATMAN-TCM: a Bioinformatics Analysis Tool for Molecular mechANism of Traditional Chinese Medicine. *Sci Rep*. 2016;6:21146. doi:10.1038/srep21146

12. Daina A, Michielin O, Zoete V. SwissTargetPrediction: updated data and new features for efficient prediction of protein targets of small molecules. *Nucleic Acids Res*. 2019;47:W357–w364. doi:10.1093/nar/gkz382
13. Stelzer G, Rosen N, Plaschkes I, et al. The GeneCards Suite: from Gene Data Mining to Disease Genome Sequence Analyses. *Curr protoc bioinf*. 2016;54:1.30.31–31.30.33. doi:10.1002/cpbi.5
14. Chen X, Ji ZL, Chen YZ. TTD: therapeutic Target Database. *Nucleic Acids Res*. 2002;30:412–415. doi:10.1093/nar/30.1.412
15. Shannon P, Markiel A, Ozier O, et al. Cytoscape: a software environment for integrated models of biomolecular interaction networks. *Genome Res*. 2003;13:2498–2504. doi:10.1101/gr.1239303
16. von Mering C, Huynen M, Jaeggi D, Schmidt S, Bork P, Snel B. STRING: a database of predicted functional associations between proteins. *Nucleic Acids Res*. 2003;31:258–261. doi:10.1093/nar/gkg034
17. Dennis G, Sherman BT, Hosack DA, et al. DAVID: database for Annotation, Visualization, and Integrated Discovery. *Genome Biol*. 2003;4:3. doi:10.1186/gb-2003-4-5-p3
18. Kanehisa M, Furumichi M, Tanabe M, et al. KEGG: new perspectives on genomes, pathways, diseases and drugs. *Nucleic Acids Res*. 2017;45: D353–d361.
19. Mills EL, Kelly B, Logan A, et al. O'Neill, Succinate Dehydrogenase Supports Metabolic Repurposing of Mitochondria to Drive Inflammatory Macrophages. *Cell*. 2016;167:457–470.e413. doi:10.1016/j.cell.2016.08.064
20. Weyand CM, Zeisbrich M, Goronzy JJ. Metabolic signatures of T-cells and macrophages in rheumatoid arthritis. *Curr Opin Immunol*. 2017;46:112–120. doi:10.1016/j.coi.2017.04.010
21. Shirai T, Nazarewicz RR, Wallis BB, et al. The glycolytic enzyme PKM2 bridges metabolic and inflammatory dysfunction in coronary artery disease. *J Exp Med*. 2016;213:337–354.
22. Xu K, Yin N, Peng M, et al. Glycolysis fuels phosphoinositide 3-kinase signaling to bolster T cell immunity. *Science*. 2021;371:405–410. doi:10.1126/science.abb2683
23. McInnes IB, Schett G. Cytokines in the pathogenesis of rheumatoid arthritis. *Nat Rev Immunol*. 2007;7:429–442.
24. Noack M, Miossec P. Selected cytokine pathways in rheumatoid arthritis. *Semin Immunopathol*. 2017;39:365–383. doi:10.1007/s00281-017-0619-z
25. McInnes IB, Buckley CD, Isaacs JD. Cytokines in rheumatoid arthritis - shaping the immunological landscape, Nature reviews. *Rheumatology*. 2016;12:63–68. doi:10.1038/nrrheum.2015.171
26. Takeuchi T, Yoshida H, Tanaka S. Role of interleukin-6 in bone destruction and bone repair in rheumatoid arthritis. *Autoimmun Rev*. 2021;20:102884. doi:10.1016/j.autrev.2021.102884
27. Chen Z, Bozec A, Ramming A, et al. Anti-inflammatory and immune-regulatory cytokines in rheumatoid arthritis, Nature reviews. *Rheumatology*. 2019;15:9–17. doi:10.1038/s41584-018-0109-2
28. McInnes IB, Schett G. *Pathogenetic Insights From the Treatment of Rheumatoid Arthritis*. *Lancet*. 2017;2328–2337.
29. Xu T, Feng G, Zhao B, et al. A non-target urinary and serum metabolomics strategy reveals therapeutical mechanism of Radix Astragali on adjuvant-induced arthritis rats. *J Chromatogr B Analyt Technol Biomed Life Sci*. 2017;1048:94–101. doi:10.1016/j.jchromb.2017.01.040
30. Bi Z, Zhao Y, Hu J, et al. A novel polysaccharide from Lonicerae Japonicae Caulis: characterization and effects on the function of fibroblast-like synoviocytes. *Carbohydr Polym*. 2022;292:119674. doi:10.1016/j.carbpol.2022.119674
31. Geng Q W, Wang S, H Q, et al. Physcion 8-O-β-glucopyranoside extracted from Polygonum cuspidatum exhibits anti-proliferative and anti-inflammatory effects on MH7A rheumatoid arthritis-derived fibroblast-like synoviocytes through the TGF-β/MAPK pathway. *Int J Mol Med*. 2018;42:745–754. doi:10.3892/ijmm.2018.3649
32. Jia P, Liu W, Liu S, et al. Therapeutic effects of Hedyotis diffusa Willd. on type II collagen-induced rheumatoid arthritis in rats. *Zhongguo Ying Yong Sheng Li Xue Za Zhi*. 2018;34:558–561. doi:10.12047/j.cjap.5665.2018.125
33. Rommel C, Camps M, Ji H. PI3K delta and PI3K gamma: partners in crime in inflammation in rheumatoid arthritis and beyond? *Nat Rev Immunol*. 2007;7:191–201. doi:10.1038/nri2036
34. Liu S, Ma H, Zhang H, et al. Recent advances on signaling pathways and their inhibitors in rheumatoid arthritis. *Clin Immunol*. 2021;230:108793. doi:10.1016/j.clim.2021.108793
35. Kim J, Jung KH, Yoo J, et al. PBT-6, a Novel PI3KC2γ Inhibitor in Rheumatoid Arthritis. *Biomol Ther (Seoul)*. 2020;28:172–183. doi:10.4062/biomolther.2019.153
36. Kanoje V, Pandey D, Wagh A, et al. Discovery and pre-clinical characterization of a selective PI3Kδ inhibitor, LL-00071210 in rheumatoid arthritis. *Eur J Pharmacol*. 2022;927:175054. doi:10.1016/j.ejphar.2022.175054
37. Shah A P, Siddique A, Thakkar S, et al. An update on novel therapeutic intervention in Rheumatoid arthritis. *Int Immunopharmacol*. 2022;109:108794. doi:10.1016/j.intimp.2022.108794
38. Chagas M, Behrens MD, Moragas-Tellis CJ, et al. Flavonols and Flavones as Potential anti-Inflammatory, Antioxidant, and Antibacterial Compounds. *Oxid Med Cell Longev*. 2022;2022:9966750. doi:10.1155/2022/9966750
39. Ren Y J, Lu Y, Qian B, et al. Recent progress regarding kaempferol for the treatment of various diseases. *Exp Ther Med*. 2019;18:2759–2776. doi:10.3892/etm.2019.7886
40. Huang L, Kim MY, Cho JY. Immunopharmacological Activities of Luteolin in Chronic Diseases. *Int J mol Sci*. 2023;24.
41. Galván-Peña S, O'Neill LA. Metabolic reprograming in macrophage polarization. *Front Immunol*. 2014;5:420. doi:10.3389/fimmu.2014.00420
42. Littlewood-Evans A, Sarret S, Apfel V, et al. GPR91 senses extracellular succinate released from inflammatory macrophages and exacerbates rheumatoid arthritis. *J Exp Med*. 2016;213:1655–1662. doi:10.1084/jem.20160061
43. Zeisbrich M, Yanes RE, Zhang H, et al. Hypermetabolic macrophages in rheumatoid arthritis and coronary artery disease due to glycogen synthase kinase 3b inactivation. *Ann Rheum Dis*. 2018;77:1053–1062. doi:10.1136/annrheumdis-2017-212647